University of Groningen

Multiple purpose algorithms for invariant manifolds

Broer, Henk; Hagen, Aaron; Vegter, Geert

Published in:
Dynamics of Continuous Discrete and Impulsive Systems. Series B: Applications & Algorithms

Publication date:
2003

MULTIPLE PURPOSE ALGORITHMS FOR INVARIANT MANIFOLDS

Henk Broer[1] Aaron Hagen[2][†] and Gert Vegter[1]

[1]Department of Mathematics and Computing Science
University of Groningen, The Netherlands
[2]Department of Mathematics
University of Texas at Arlington, TX 76019

Abstract. This paper deals with the numerical continuation of invariant manifolds, regardless of the restricted dynamics. Typically, invariant manifolds make up the skeleton of the dynamics of phase space. Examples include limit sets, co-dimension 1 manifolds separating basins of attraction (separatrices), stable/unstable/center manifolds, nested hierarchies of attracting manifolds in dissipative systems and manifolds in phase plus parameter space on which bifurcations occur. These manifolds are for the most part invisible to current numerical methods. The approach is based on the general principle of normal hyperbolicity, where the graph transform leads to the numerical algorithms. This gives a highly multiple purpose method. Examples of computations of both attracting and saddle-type (1D and 2D) manifolds will be given, with and without non-uniform adaptive refinement. A convergence result for the algorithm will be sketched.

Keywords. Invariant manifolds, normal hyperbolicity, chaotic dynamics, numerical continuation, bifurcation theory, computational geometry, graph transform.

AMS (MOS) subject classification: 34C28, 34C30, 34C45, 37D10, 37M99, 65D18, 65L99, 65P30, 70K50

1 Introduction

Invariant manifolds of dynamical systems largely determine the geometry of their phase space. Codimension 1 manifolds, for example, may separate basins of attraction. But in general equilibria, closed curves, invariant tori, their stable and unstable manifolds etc. are the corner stones around which a more detailed analysis may be in order. If the invariant manifold of interest, say Σ_1, is no attractor, it may still lie in a higher dimensional invariant manifold, Σ_2, which is. If the dynamics are restricted to Σ_2 then Σ_1 may even serve as a separatrix. This is the kind of situation we want to look at in the present paper. To fix thoughts think of Σ_2 being a 3–torus attractor

with phase lock dynamics, where the aim is to visualize an unstable 2–torus Σ_1 inside this 3–torus.

The key notion needed here is *normal hyperbolicity* of the invariant manifold, which guarantees the smooth persistence of the manifold under small perturbations of the system. This persistence property enables us to develop *robust* numerical algorithms that compute these manifolds by numerical continuation. At each step of the continuation process we use the *graph transform* to find the new 'perturbed' invariant manifold. The graph transform is a classical tool for proving the invariant manifold theorem (see Section 2.1). This transform is a contraction on a Banach space of functions, whose graph is near the invariant manifold. The fixed point of the graph transform corresponds to the invariant manifold itself. See [9] for details.

Simple iteration of a dynamical system has been used a lot in the literature to visualize invariant manifolds. However, in general it is impossible to numerically locate an invariant manifold by iteration, even in the case of a normally hyperbolic attractor. The reason is that the manifold may contain smaller attractors, like in the case of Σ_2. Our method is independent of the dynamics on the manifold and can in principal be used to compute Σ_2.

Another advantage of our method can be explained by the example of Σ_2. Now finding the separatrix 2–torus Σ_1 within Σ_2 is hardly possible by simple iteration. Indeed, the numerical errors grow exponentially in the unstable direction. However, since Σ_1 in the ambient space is normally hyperbolic of saddle–type, our methods apply and we can visualize this object. In fact, our approach will reverse this numerical instability, effectively making Σ_1 a stable object. We emphasize that the algorithm converges whether the dynamics on Σ_1 is quasi-periodic or more complicated, regardless.

The computation of invariant manifolds of higher dimension has been addressed in the literature previously. Dieci and Lorenz [5] developed a method to compute normally hyperbolic attracting tori. Their approach requires global parametrizations of the tori. The method employs the graph transform, and a convergence result is given in which the discretized graph transform is a contraction. Broer, Osinga, and Vegter [3] present a method to compute normally hyperbolic invariant manifolds of saddle–type. They use simplicial complexes with flat faces to approximate manifolds. Since the manifold is of saddle–type, the invariant stable/unstable splitting is computed as a prerequisite to iterating the graph transform.

Three general aspects distinguish the present paper from previous attempts. The first involves the discretization of the manifold. The approach here approximates the manifold locally using polynomial maps from the tangent space to the normal space. This gives a non-uniform approximation of arbitrary order for any manifold. The second difference is in the choice of coordinates in the neighborhood of the manifold. Briefly, our choice results in smooth coordinates, an a-priori dimension reduction and an improvement in contraction rate. The third aspect regards the convergence result. Computational experiments indicate the algorithm is contractive even in the absence

of normal hyperbolicity. Normal exponential attraction is enough. To explain this, a convergence result is given, where we obtain the expected order of approximation for the computed manifold, and that the discretized graph transform is a contraction, without the hypothesis of normal hyperbolicity. The reason this works is the following. To iterate our procedure, the discretized graph transform Γ_D must preserve the bound on the Lipschitz norm of a section. The essential difficulty is that given a function bounded only in Lipschitz norm, there is not a very good bound on the Lipschitz constant of its interpolant. The estimate that we use comes from the observation that as the C^0 norm of a function goes to zero, the Lipschitz norm of its interpolant goes to zero, for a fixed mesh size.

2 Normal hyperbolicity and the invariant manifold theorem

This section reviews part of the theory of normally hyperbolic manifolds and paves the way for the development of an efficient algorithm for their computation. First we present an overview of some basic definitions and results from [9]. Consider a C^r diffeomorphism F on $\mathbb{R}^n$, having an r–normally hyperbolic invariant manifold $\Sigma \subset \mathbb{R}^n$. Recall that Σ is r–normally hyperbolic for F, $r \geq 1$, if there is a continuous DF–invariant splitting

$$T_\Sigma(\mathbb{R}^n) = N^u(\Sigma) \oplus T(\Sigma) \oplus N^s(\Sigma), \tag{1}$$

and a Riemann structure on the tangent bundle $T_\Sigma(\mathbb{R}^n)$, such that, for $y \in \Sigma$, $i \geq 0$, and $0 \leq k \leq r$:

$$\begin{aligned}
\| DF^i \, | \, N_y^s(\Sigma) \| \cdot \| (DF^i \, | \, T_y(\Sigma))^{-1} \|^k &\leq c\mu^i, \\
\| (DF^i \, | \, N_y^u(\Sigma))^{-1} \| \cdot \| DF^i \, | \, T_y(\Sigma) \|^k &\leq c \, (1/\lambda)^i,
\end{aligned} \tag{2}$$

for some $0 < \mu < 1 < \lambda < \infty$, $0 < c < \infty$. Here the operator norms are associated with the Riemann structure on $T_\Sigma(\mathbb{R}^n)$.

According to the *Invariant Manifold Theorem* [9, Theorem 4.1], a C^r diffeomorphism $\tilde{F}$, that is C^r–near F, has an r–normally hyperbolic invariant manifold $\tilde{\Sigma}$, that is C^r and C^r–near Σ. Our primary goal is the computation of $\tilde{\Sigma}$. To compute $\tilde{\Sigma}$, we look at the classical proof for its existence. The manifold $\tilde{\Sigma}$ is constructed in a vector bundle $N(\Sigma)$ transverse to $T(\Sigma)$. The invariant splitting (1) induces a splitting of this transverse bundle into stable and unstable parts, $N(\Sigma) = N^u(\Sigma) \oplus N^s(\Sigma)$. The *hyperbolic splitting* $N^u(\Sigma) \oplus T(\Sigma) \oplus N^s(\Sigma)$ has all the growth properties of the invariant splitting (1). The graph transform is then defined in terms of this hyperbolic splitting. A natural choice for $N(\Sigma)$ is given by the invariant splitting (1). One drawback is that this $N(\Sigma)$ is not necessarily Lipschitz, so may not yield smooth coordinates of a neighborhood of Σ.

Our approach will be to construct $\tilde{\Sigma}$ in the orthogonal bundle $N(\Sigma)$, that is, the bundle whose fiber at a point $y \in \Sigma$ is the orthogonal complement in $T_y(\mathbb{R}^n)$ of $T_y(\Sigma)$, with respect to the Euclidean norm. This bundle has one degree of smoothness less than Σ. Also, $N(\Sigma)$ is a-priori known (it is given by Σ), unlike the transverse bundle invariant under DF. A third benefit of $N(\Sigma)$ is an improved contraction rate for the linear graph transform updating the hyperbolic splitting. The problem of determining the hyperbolic splitting is a-priori restricted to $N(\Sigma)$. Hence, only the stable and unstable growth rates enter the picture, not the tangent growth rate. From now on, by the notation $N(\Sigma) = N^u(\Sigma) \oplus N^s(\Sigma)$ we mean any given transverse bundle. In computations, $N(\Sigma)$ will be an approximation of the orthogonal bundle.

To formulate the graph transform in a way suitable for a numerical algorithm, we need a concrete representation of the hyperbolic splitting $N^u(\Sigma) \oplus T(\Sigma) \oplus N^s(\Sigma)$. To this end, let $P^s(y) : \mathbb{R}^n \to \mathbb{R}^n$ denote the projection matrix with range $N_y^s(\Sigma)$ and nullspace $T_y(\Sigma) \oplus N_y^u(\Sigma)$, let $P^u(y) : \mathbb{R}^n \to \mathbb{R}^n$ denote the projection matrix with range $N_y^u(\Sigma)$ and nullspace $T_y(\Sigma) \oplus N_y^s(\Sigma)$, and let $Q(y) : \mathbb{R}^n \to \mathbb{R}^n$ denote the orthogonal projection matrix with range $T_y(\Sigma)$. In practice, the projections are calculated using orthonormal moving frames spanning $N^u(\Sigma)$, $N^s(\Sigma)$, and $T(\Sigma)$ in $T_\Sigma(\mathbb{R}^n)$.

In overview, one step of our continuation algorithm has two parts. The initial data is an F–invariant manifold Σ with its hyperbolic splitting $N^u(\Sigma) \oplus T(\Sigma) \oplus N^s(\Sigma)$. The first step uses the graph transform on Σ with $N^u(\Sigma) \oplus T(\Sigma) \oplus N^s(\Sigma)$ to determine the $\tilde{F}$–invariant manifold $\tilde{\Sigma}$. The second step uses the *linear graph transform* $\mathcal{L}$ together with initial data determined by $\tilde{\Sigma}$ and $N^u(\Sigma) \oplus T(\Sigma) \oplus N^s(\Sigma)$ to determine the hyperbolic splitting $N^u(\tilde{\Sigma}) \oplus T(\tilde{\Sigma}) \oplus N^s(\tilde{\Sigma})$ of $\tilde{\Sigma}$. Now the first and second steps may be repeated with initial data $\tilde{\Sigma}$ and $N^u(\tilde{\Sigma}) \oplus T(\tilde{\Sigma}) \oplus N^s(\tilde{\Sigma})$. In fact there are two linear graph transforms $\mathcal{L}^s$ and $\mathcal{L}^u$ which locate $N^s(\tilde{\Sigma})$ and $N^u(\tilde{\Sigma})$, respectively. For example, $\mathcal{L}^s$ operates on a space of j–plane bundles near $N^s(\Sigma)$ in $T_\Sigma(\mathbb{R}^n)$, where $j = \dim N^s(\Sigma)$. The linear graph transform $\mathcal{L}^s$ is a contraction on this space with fixed point $N^s(\tilde{\Sigma})$. This is elaborated in [2].

3   The graph transform

In this section a concrete formulation of the graph transform is given, which will be used to develop an algorithm for the invariant manifold. The manifold $\Sigma \subset \mathbb{R}^n$ is a C^1 compact boundaryless manifold, F–invariant, r–normally hyperbolic, $r \geq 1$, with splitting $N^u(\Sigma) \oplus T(\Sigma) \oplus N^s(\Sigma)$. Here, $N^u(\Sigma) \oplus N^s(\Sigma) = N(\Sigma)$ is any bundle transverse to $T(\Sigma)$, where $N_y^s(\Sigma)$ (resp. $N_y^u(\Sigma)$), $y \in \Sigma$, are Lipschitz continuous functions $\Sigma \to G_{n,j}$. Here, $G_{n,j}$ is the Grassmann manifold of j–planes of $\mathbb{R}^n$, where $j = \dim N^s(\Sigma)$ (resp. $N^u(\Sigma)$). We refer to $N^s(\Sigma)$ as the *stable bundle* and to $N^u(\Sigma)$ as the *unstable bundle*.

Under these assumptions, $N(\Sigma)$ induces a tubular neighborhood U of Σ, [8]. In fact, U is lipeomorphic to $\{(p, v) : p \in \Sigma, v \in N_p(\Sigma), |v| < \epsilon\}$ for
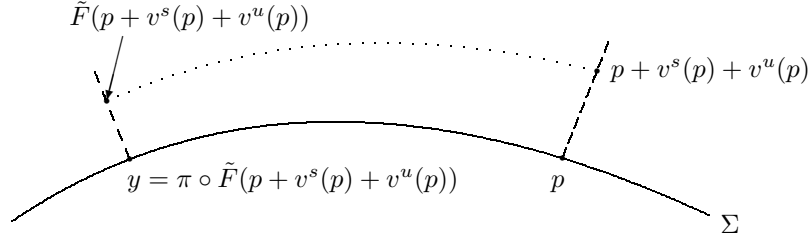
Figure 1: Invariance Condition

some $\epsilon > 0$. The point $(p, v) \in N(\Sigma)$ corresponds to the point $p + v \in U$. From now on we take $N(\Sigma) = \{(p, v) : p \in \Sigma, v \in N_p(\Sigma), |v| < \epsilon\}$, and do not distinguish between $N(\Sigma)$ and the neighborhood U of Σ. For each $y \in U$, there is a unique fiber of $N(\Sigma)$ through y, say $N_p(\Sigma)$. The projection of y onto Σ is $\pi(y) = p \in \Sigma$. The vector $y - \pi(y)$, being in $N_{\pi(y)}(\Sigma)$, may be decomposed uniquely as $y - \pi(y) = v^s + v^u$, $v^s \in N_{\pi(y)}^s(\Sigma)$ and $v^u \in N_{\pi(y)}^u(\Sigma)$. Hence, any point y in U may be written $y = \pi(y) + v^s + v^u$.

We look for an $\tilde{F}$–invariant manifold $\tilde{\Sigma}$ in the neighborhood U of Σ. Now, $\tilde{\Sigma}$ will be represented as a graph in $N^s(\Sigma)$ plus a graph in $N^u(\Sigma)$. Thus, suppose that $\mathcal{S}_{\epsilon,\delta}^s$ is the space of Lipschitz sections of $N^s(\Sigma)$ with Lipschitz constant less than δ, [6, 9], where ϵ is the diameter of the tubular neighborhood U. Similarly define $\mathcal{S}_{\epsilon,\delta}^u$. Elements of $\mathcal{S}_{\epsilon,\delta}^s$ are Lipschitz maps $\sigma^s : \Sigma \to N^s(\Sigma)$, and we write $\sigma^s(p) = (p, v^s(p))$, for some $v^s(p) \in N_p^s(\Sigma)$. The notation for $\mathcal{S}_{\epsilon,\delta}^u$ is analogous. The space $\mathcal{S}_{\epsilon,\delta}^s$ ($\mathcal{S}_{\epsilon,\delta}^u$) with the natural C^0 norm on sections, denoted $|\cdot|_b$, is complete. Now define $\mathcal{S}_{\epsilon,\delta}$ to be the set of all pairs of sections (σ^s, σ^u) with $\sigma^s \in \mathcal{S}_{\epsilon,\delta}^s$, and $\sigma^u \in \mathcal{S}_{\epsilon,\delta}^u$. The space $\mathcal{S}_{\epsilon,\delta}$ is complete with respect to the norm $\|(\sigma^s, \sigma^u)\| \equiv \max\{|\sigma^s|_b, |\sigma^u|_b\}$.

If $\sigma = (\sigma^s, \sigma^u) \in \mathcal{S}_{\epsilon,\delta}$, $\sigma^s(p) = (p, v^s(p))$ and $\sigma^u(p) = (p, v^u(p))$, then

$$\text{graph}\{\sigma\} \equiv \{p + v^s(p) + v^u(p) : p \in \Sigma\} \tag{3}$$

is a Lipschitz manifold near Σ in Lipschitz norm for small ϵ, δ.

We may split the $\tilde{F}$–invariance condition $\text{graph}\{\sigma\} = \tilde{F}(\text{graph}\{\sigma\})$ into two coupled equations, a part on Σ and a part normal to Σ. That is, $\{p + v^s(p) + v^u(p) : p \in \Sigma\}$ is $\tilde{F}$–invariant if and only if

$$\begin{aligned} v^s(y) + v^u(y) &= \tilde{F}(p + v^s(p) + v^u(p)) - y, \\ y &= \pi \circ \tilde{F}(p + v^s(p) + v^u(p)), \end{aligned} \tag{4}$$

for $p \in \Sigma$. See Figure 1. Under our hypotheses, $y = \pi \circ \tilde{F}(p + v^s(p) + v^u(p))$ may be solved for $p \in \Sigma$ given $y \in \Sigma$, $\sigma^s \in \mathcal{S}_{\epsilon,\delta}^s$ and $\sigma^u \in \mathcal{S}_{\epsilon,\delta}^u$ for small ϵ, δ, and $\theta \equiv \|F - \tilde{F}\|_{C^1}$. Denote this solution by $p = p(y, v^s, v^u)$.

The *graph transform* is a map $\Gamma : \mathcal{S}_{\epsilon,\delta} \to \mathcal{S}_{\epsilon,\delta}$ given by a pair $\Gamma(\sigma) \equiv (\Gamma^s(\sigma), \Gamma^u(\sigma))$, for $\sigma \in \mathcal{S}_{\epsilon,\delta}$. Putting $\Gamma^s(\sigma)(p) \equiv (p, w^s(p))$, we define $w^s(p)$,

by multiplying the first equation of (4) by $P^s(y)$,

$$w^s(y) = P^s(y) \left[\tilde{F}(p + v^s(p) + v^u(p)) - y \right], \; p = p(y, v^s, v^u), \qquad (5)$$

for $y \in \Sigma$.

Putting $\Gamma^u(\sigma)(p) \equiv (p, w^u(p))$, and by multiplying the first equation of (4) by $P^u(y)$, we define $w^u(p)$, for $p \in \Sigma$, implicitly from the relationship

$$\begin{aligned} v^u(y) &= P^u(y) \left[\tilde{F}(p + v^s(p) + w^u(p)) - y \right], \\ y &= \pi \circ \tilde{F}(p + v^s(p) + w^u(p)), \end{aligned} \qquad (6)$$

for $p \in \Sigma$. In (6), there is a unique solution for $w^u(p)$ for small θ, ϵ, and δ.

If $(\sigma^s, \sigma^u) = (\Gamma^s(\sigma), \Gamma^u(\sigma))$, then (5) and (6) imply (4), and hence the graph of (σ^s, σ^u) is $\tilde{F}$–invariant. Hence σ is a fixed point of Γ if and only if the graph of σ is an $\tilde{F}$–invariant manifold.

To insure that Γ is a contraction under the condition of (eventual) r–normal hyperbolicity (2), it may be necessary to replace $\tilde{F}$ with $\tilde{F}^N$, some large integer N, in the definition of Γ above. This is a standard step in the classical proof of the Invariant Manifold Theorem [6, 9]. With this replacement, we have the main theorem concerning the existence of $\tilde{\Sigma}$ obtained as the graph of the fixed point of Γ, [6, 9, 11, 12].

Theorem 1 *Let $F, \tilde{F} : \mathbb{R}^n \to \mathbb{R}^n$ be C^r maps for some $r \geq 1$. Suppose $\Sigma \subset \mathbb{R}^n$ is a compact boundaryless manifold of class C^1. Also, suppose Σ is F–invariant, r–normally hyperbolic, and that $F|_\Sigma$ is a diffeomorphism.*

Then there exists $\theta > 0$ such that, if $\|F - \tilde{F}\|_{C^r} < \theta$, there exists a C^r manifold $\tilde{\Sigma}$, C^r close to Σ, $\tilde{F}$–invariant and r–normally hyperbolic.

Moreover, suppose $N_p^u(\Sigma), N_p^s(\Sigma)$ are Lipschitz functions of $p \in \Sigma$, and Γ is the graph transform defined above. Then there exists $\theta, \epsilon, \delta > 0$, such that $\Gamma : \mathcal{S}_{\epsilon,\delta} \to \mathcal{S}_{\epsilon,\delta}$ is a contraction whose fixed point has graph equal to $\tilde{\Sigma}$.

Remark 1 The case that F is one or more steps of a time discretization falls into the framework of Sections 2 and 3, [7]. Thus the results of this paper apply to vector fields as well as maps.

4 Algorithm for the Invariant Manifold

In Sections 2 and 3 we discussed the graph transform in a setting suitable for computations. This involved the choice of an appropriate hyperbolic splitting, and explicit formulas for the graph transform. This section gives a computable approximation of any manifold $\tilde{\Sigma}$ which is C^1–near the initial manifold Σ. This leads to an algorithm for approximating $\tilde{\Sigma}$, obtained by applying the graph transform to these *discrete manifolds*.

To discretize $\tilde{\Sigma}$, initial data consisting of a C^1 compact manifold $\Sigma \subset \mathbb{R}^n$, with a Lipschitz transverse bundle $N(\Sigma) = N^s(\Sigma) \oplus N^u(\Sigma)$ are required. This scheme gives an approximation of order $p \geq 1$ for $\dim \Sigma \equiv d \geq 1$.

The first component of the discrete manifold is a d–dimensional simplicial complex $\mathcal{C}$ in $\mathbb{R}^n$ with vertices in Σ. The d–simplices of $\mathcal{C}$ will be denoted by $\mathcal{C}_1, \ldots, \mathcal{C}_m$. The maximal diameter of the d–simplices of $\mathcal{C}$ will be denoted $H > 0$, and the polyhedron determined by $\mathcal{C}$ by Σ_H^P. We assume that Σ_H^P is a d–dimensional manifold in $\mathbb{R}^n$ homeomorphic to Σ. In this case we say that $\mathcal{C}$ *supports* Σ. It is well known that every compact submanifold of $\mathbb{R}^n$ has a supporting simplicial complex. Note that since $\Sigma \in C^1$, we have $\mathrm{dist}\left(\Sigma_H^P, \Sigma\right) = o(H)$, as $H \to 0$. The family of sets $\{\mathcal{C}_i\}_{i=1}^m$, with the associated parameter H, must be a *regular family* [4]. Roughly, this means none of the $\mathcal{C}_i$ are almost contained in a $(d-1)$–dimensional hyperplane, uniformly as $H \to 0$. The second component is the *principal lattice of order p* of each d–simplex $\mathcal{C}_k$, [4]. For instance, in the case of the standard 2–simplex, the positions of the points of the principal lattice of order p are given by the first $p+1$ rows of Pascal's triangle. The points of the lattice are called the 'nodes' of $\mathcal{C}_k$.

The third component is a discrete representation of the stable and unstable bundles of Σ, $N^s(\Sigma)$ and $N^u(\Sigma)$. For this we must assume H is small enough that $N(\Sigma)$ is transverse to Σ_H^P. Then $N(\Sigma)$ induces a one-to-one correspondence between points $y \in \Sigma_H^P$ and $u \in \Sigma$. Now we approximate $N^s(\Sigma)$ and $N^u(\Sigma)$ by bundles over Σ_H^P. The initial data for the approximation consists of the fibers at the vertices of each $\mathcal{C}_k$. These are then interpolated as functions over each $\mathcal{C}_k$. The interpolated $N(\Sigma)$ are globally Lipschitz and transverse to $T(\Sigma)$, hence induce a tubular neighborhood. See [1,2] for details.

The fourth and final component is, for each $\mathcal{C}_k$, a point in each of the stable and unstable fibers at each node. At a node, the sum of these two points is the intersection of $\tilde{\Sigma}$ with the normal fiber. The points of intersection of $\tilde{\Sigma}$ with the normal fibers at the nodes are called the 'grid points'. For each $\mathcal{C}_k$, the stable (unstable) points determine a stable (unstable) polynomial. We use the coordinates induced by $N^s(\Sigma)$ (resp. $N^u(\Sigma)$) to reduce the problem of interpolating the stable (unstable) points to one involving functions $\mathcal{C}_k \to \mathbb{R}^j$, where $j = \dim N^s(\Sigma)$ (resp. $N^u(\Sigma)$). Then, in coordinates, the polynomials are the pth order Lagrange polynomials on the d–simplex $\mathcal{C}_k$, [4]. Locally, the discrete manifold approximating $\tilde{\Sigma}$ is the sum of graphs of stable and unstable polynomials defined on $\mathcal{C}_k$. This discrete manifold, $\tilde{\Sigma}_D$, is a pth order approximation to $\tilde{\Sigma}$, as $H \to 0$.

A discrete version Γ_D of the graph transform Γ may now be defined. Conceptually, there is no difference between the derivation of the discrete graph transform Γ_D and the derivation of Γ in Section 3. Using Σ_H^P in place of the initial manifold Σ and using the discrete normal fibers and the discrete manifolds $\tilde{\Sigma}_D$ for the candidate manifolds near Σ, one derives Γ_D just as Γ was derived. See [1,2] for details.
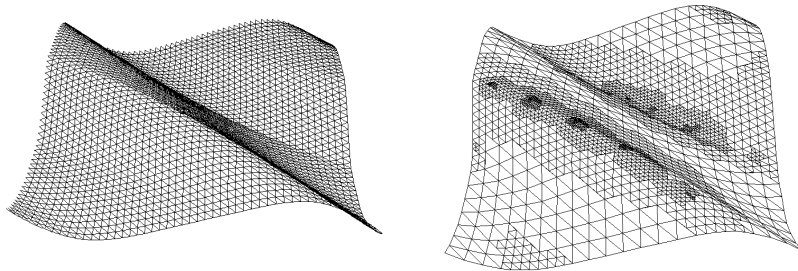
Figure 2: Invariant torus of fattened Thom map, losing smoothness, $\epsilon = 0.6$; left: 5000 third order elements, right: first order adaptively refined

5   Computations

This section contains some of the numerical experiments done to test the performance of our algorithm. In Section 6, we will propose a mathematical mechanism for the observed convergence of the algorithm.

These examples illustrate different features and benefits of our approach. To demonstrate that the algorithm converges regardless of the dynamics on the manifold, examples were chosen with a wide variety of dynamics. The first three examples are computations of invariant tori. In the first torus there is a dense intersection of the stable and unstable manifolds of a saddle point. In the second torus, there are two saddle points, a source, and a sink – almost all the points on the torus are in the basin of attraction of the sink. The third is a quasiperiodic torus of a vector field, which may be phase-locked depending on the value of the continuation parameter. The last two examples are saddle–type invariant curves. In the first of these there is a range of dynamics as the continuation parameter varies: initially quasiperiodic with phase locking, then a saddle–node bifurcation. The second is a saddle–type periodic orbit of a vector field. No special difficulty was ever observed in the continuation due to these different dynamical scenarios.

Another advantage of our approach is illustrated in Examples 1 and 2. In these examples, continuation is carried out past the point where normal hyperbolicity of the torus is lost. As indicated earlier, contractivity of Γ_D is retained because the tori remain attractive. Thus, it is possible to see how the tori lose their smoothness as the parameter varies. An additional feature is highlighted in the computations involving vector fields, Examples 3 and 5. In both cases, initial data is obtained by simulation, and is quite rough. Here, Γ_D converged with this rough initial data, smoothing it out. The examples also illustrate that Γ_D remains contractive for different values of $p \geq 1$ and a non–uniform mesh. Example 1 uses $p = 3$ and a non–uniform mesh, and Example 4 uses $p = 3$. Additionally, in Examples 1 and 4, comparisons are made to computations in [3]. Here, we are able to carry continuation farther due to the choice of the hyperbolic splitting mentioned earlier.
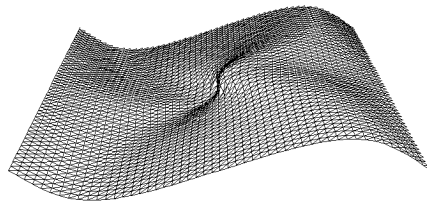
Figure 3: Invariant torus of a fattened 'sink' map, losing smoothness, $\epsilon = 0.4$; 5000 first order elements

Example 1: The $3D$ fattened Thom map

$$\begin{array}{rcl} x_{i+1} & = & 0.1x_i + \epsilon \sin z_i \\ y_{i+1} & = & z_i + y_i + \epsilon x_i \\ z_{i+1} & = & 2z_i + y_i + \epsilon x_i \end{array} \quad , \quad (x_i, y_i, z_i) \in \mathbb{R} \times \mathbf{S}^1 \times \mathbf{S}^1 \qquad (7)$$

For (7) with $\epsilon = 0$, $x = 0$ is an attracting torus. The torus loses hyperbolicity at $\epsilon = 0.47$, although it is still attracting. Starting from $\epsilon = 0.0$, we set $\epsilon = 0.3$ and iterated to the invariant torus. This took 5 iterates, with average contraction 0.1179. This is close to 0.1, which is what we expect from (7). Taking ϵ steps of 0.02, we continued the torus to $\epsilon = 0.6$, see Figure 2. The second computation with example (7) used adaptive refinement. We started with 800 first order elements. After each iteration, elements whose tangent data differed significantly from neighboring elements' tangent data were subdivided. Taking ϵ steps of 0.02, we continued the torus to $\epsilon = 0.6$. The average contraction was 0.12, and the final torus, illustrated in Figure 2, has 4652 elements. For $\epsilon \approx 0.47$, the shape of our torus is the same as that computed in [3]. Indeed, the shape of the $\epsilon = 0.6$ torus is near that of the $\epsilon \approx 0.47$ torus, except that there appears to be a ridge along which the torus is losing smoothness, see Figure 2. In fact, there is small scale bumpiness along the ridge of the torus on the right in Figure 2, and this area is the site of a further loss of smoothness for increasing ϵ.

Example 2: A fattened 'sink' map

$$\begin{array}{l} x_{i+1} = 0.25x_i + \epsilon \sin z_i \\ y_{i+1} = y_i + 0.5 \sin y_i + \epsilon x_i \\ z_{i+1} = z_i - 0.5 \cos y_i \sin z_i + \epsilon x_i \end{array} \quad , \quad (x_i, y_i, z_i) \in \mathbb{R} \times \mathbf{S}^1 \times \mathbf{S}^1 \qquad (8)$$

For (8) with $\epsilon = 0$, $x = 0$ is an attracting torus. At $\epsilon = 0.13$, the torus loses hyperbolicity at a sink. For $\epsilon > 0.13$, the sink has two stable complex conjugate eigenvalues whose eigenspace is a plane normal to the torus. We continued the torus to $\epsilon = 0.4$ using ϵ steps of 0.1. The average contraction through the first two continuation steps was 0.2649, close to 0.25. In Figure 3, the influence of the linear behaviour at the sink is evident in the shape of the torus as it appears to lose smoothness.
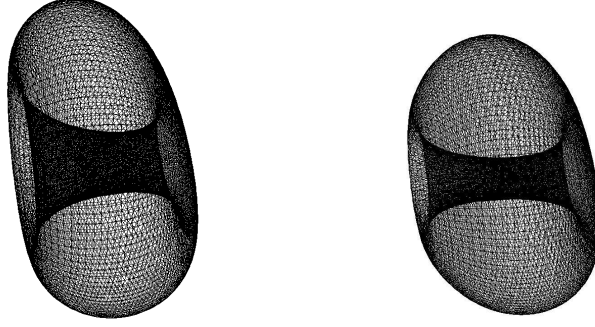
Figure 4: Lorenz-84 invariant tori, near Hopf saddle–node bifurcation; 32768 first order elements; left: $F = 1.84$, right: $F = 1.755$

Example 3: The 'Lorenz-84' system, [13]

$$
\begin{aligned}
\dot{x} &= -y^2 - z^2 - 0.25x + 0.25F \\
\dot{y} &= xy - 4xy - y + G \qquad , \quad (x, y, z) \in \mathbb{R}^3 \qquad (9) \\
\dot{z} &= 4xy + xz - z
\end{aligned}
$$

System (9) exhibits a Hopf saddle–node bifurcation near $(F, G) = (1.68, 1.68)$, [10]. There is a repelling torus in a region 'above' this point in parameter space. We continued the torus along a segment with G fixed, $\Delta F = 0.01$, towards and away from the Hopf saddle–node point. The initial torus was an approximation to the torus for $(F, G) = (1.8, 1.65)$. Figure 4 shows the two final tori computed, for $F = 1.84$ and $F = 1.755$. At this point, computational instability was observed, although the torus continues to exist, for increasing and decreasing F. This instability may be due to insufficient numerical resolution and weak attraction. Note for decreasing F the torus approaches a more sphere–like surface and the inner radius gets smaller. This is expected since the parameters approach the Hopf saddle–node point.

Example 4: The $3D$-fattened Arnold family

$$
\begin{aligned}
x_{i+1} &= x_i + 0.1 + \epsilon(y_i + z_i/2 + \sin x_i) \\
y_{i+1} &= 0.3(y_i + \sin x_i) \qquad , \quad (x_i, y_i, z_i) \in \mathbf{S}^1 \times \mathbb{R}^2 \qquad (10) \\
z_{i+1} &= 2.4(y_i + z_i + \sin x_i)
\end{aligned}
$$

For $\epsilon = 0$, (10) has a closed curve of saddle–type. We continued the curve to $\epsilon = 0.78$, near where the curve loses hyperbolicity at a sink. The initial invariant curve and hyperbolic splitting was analytically known. Here, $\Delta\epsilon = 0.2$, and the last ϵ value for which the hyperbolic splitting was computed was 0.6. Figure 5 shows the final curve with its hyperbolic splitting – the angle between the stable and unstable parts of which is small. Similar results were obtained in [3], where the curve was continued to $\epsilon = 0.7125$.
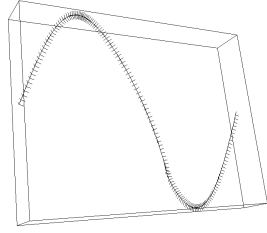
Arnold family curve with nearly degenerate hyperbolic splitting, $\epsilon = 0.78$; 50 third order elements
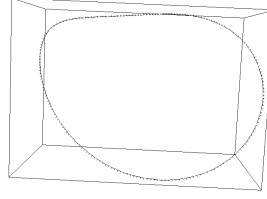
Lorenz system curve near a homoclinic orbit, $r = 16.5$; 200 first order elements

Figure 5: Saddle–type invariant curves

Example 5: The Lorenz system, [14]

$$\begin{array}{rcl}
\dot{x} & = & 10(y - x) \\
\dot{y} & = & rx - y - xz \quad , \quad (x, y, z) \in \mathbb{R}^3 \\
\dot{z} & = & xy - (8/3)z
\end{array} \tag{11}$$

At $r = 20.0$, (11) has a saddle–type periodic orbit, which was continued to $r = 16.5$. Figure 5 shows the final curve near a homoclinic orbit. In this example it was necessary to redistribute the grid points near the sharp bend in the curve to prevent their spread during continuation.

6 Convergence of the Algorithm

In Section 3 the usual formulation of the graph transform was derived. In Section 4 discrete manifolds were introduced. Then Γ_D arose from considering the graph transform acting on discrete manifolds. Now we show that Γ_D is a contraction on a suitable space of functions. Thus the algorithm converges to a discrete manifold $\tilde{\Sigma}_D$. Also, if $\tilde{\Sigma}$ is sufficiently smooth, then $\tilde{\Sigma}_D$ is a pth order approximation to $\tilde{\Sigma}$ as $H \to 0$. In this section we give a heuristic explanation of the convergence result. See [1] for details.

One step of Γ_D differs from one step of Γ in two ways. First, the stable/unstable and normal/tangent fibers used to define Γ are replaced by approximations of these fibers. With this replacement, we stay within the limits of the usual formulation of Γ. This is because our fiber approximations are Lipschitz and have appropriate transversality properties. Second, after the usual graph transform procedure, the resulting manifold is interpolated. Hence, we may write the discrete graph transform as $\Gamma_D = I_p \circ \Gamma$. Here, Γ is the usual graph transform (defined using the approximate stable/unstable and normal/tangent fibers), and I_p is the pth order interpolation of manifolds described in Section 4.

Under the assumption of normal hyperbolicity, Γ is a contraction on the space of sections $\mathcal{S}_{\epsilon, \delta}$. A look at the proof of this $[6, 9, 15]$ reveals three

steps. (To simplify the discussion, assume that Σ is attracting.) First, for any section σ bounded by ϵ, the section $\Gamma \circ \sigma$ is bounded by ϵ. This is proved using only the attraction toward the manifold, by choosing ϵ and $\theta \equiv \|F - \tilde{F}\|_{C^1}$ small. Second, for any section σ bounded by ϵ with Lipschitz constant bounded by δ, the Lipschitz constant of $\Gamma \circ \sigma$ is bounded by δ. This is proved using the normal hyperbolicity of Σ by choosing ϵ, δ, and θ small. Third, the Lipschitz constant of $\Gamma : \mathcal{S}_{\epsilon,\delta} \to \mathcal{S}_{\epsilon,\delta}$ is less than one. To prove this, one uses the attraction towards the manifold and the fact that Γ preserves the bound ϵ and the Lipschitz constant δ of sections. Again, one chooses ϵ, δ, and θ small.

Can we show that $\Gamma_D = I_p \circ \Gamma$ is a contraction on a space of sections similarly? Consider the first step above. On each simplex of Σ_H^P, I_p is Lagrange interpolation. So, given a section σ bounded by ϵ, $I_p \circ \sigma$ is a section bounded by $C_p \epsilon$, some $C_p \geq 1$. For a section σ bounded by ϵ, $\Gamma \circ \sigma$ is bounded by $\alpha \epsilon$, some $\alpha \in (0, 1)$, for ϵ and θ small. In fact, α is the factor of contraction towards Σ under F. Thus, by replacing F with F^N if necessary (as in Section 3), we may make $\alpha > 0$ smaller than $1/C_p$. Then for any section σ bounded by ϵ, $I_p \circ \Gamma \circ \sigma$ is bounded by $C_p \alpha \epsilon < \epsilon$. Now consider the second step above. If σ is a section bounded by ϵ, $\Gamma \circ \sigma$ is bounded by $\alpha \epsilon$ and hence the Lipschitz constant of $I_p \circ \Gamma \circ \sigma$ is bounded by $C_p' \alpha \epsilon / H$, some $C_p' > 0$. We will choose ϵ/H sufficiently small that $C_p' \alpha \epsilon / H < \delta$. In this way we obtain that Γ_D carries the space of sections $\mathcal{S}_{\epsilon,\delta}$ into itself. Now consider the third step above. We have $\mathrm{Lip}\{\Gamma_D\} \leq \mathrm{Lip}\{I_p\}\mathrm{Lip}\{\Gamma\}$. Due to the linearity properties of Lagrange interpolation, $\mathrm{Lip}\{I_p\} \leq C_p$. A look at the third step above reveals $\mathrm{Lip}\{\Gamma\} \leq \alpha + o(1)$ as $\epsilon + \delta + \theta \to 0$. Hence $\mathrm{Lip}\{\Gamma_D\} \leq C_p \alpha + o(1)$ as $\epsilon + \delta + \theta \to 0$. Since $C_p \alpha < 1$, we obtain $\mathrm{Lip}\{\Gamma_D\} < 1$ for small ϵ, δ, and θ. Following this outline we conclude $\Gamma_D : \mathcal{S}_{\epsilon,\delta} \to \mathcal{S}_{\epsilon,\delta}$ is a contraction for suitably chosen ϵ, δ, θ, and H.

The final part of the convergence result regards the approximation properties of the fixed point of Γ_D. If $\tilde{\Sigma}_D$ is the graph of the fixed point of Γ_D and $\tilde{\Sigma}$ is the graph of the fixed point of Γ, then $\tilde{\Sigma}_D$ is a pth order approximation to $\tilde{\Sigma}$, as $H \to 0$, provided $\tilde{\Sigma} \in C^{p+1}$. This is a consequence of the standard error estimate for Lagrange interpolation.

The essential hypotheses of this result are: (1) There exists a smooth manifold Σ, exponentially attracting and F–invariant. (2) There exists a smooth manifold $\tilde{\Sigma}$, $\tilde{F}$–invariant and C^1–near Σ. Normal hyperbolicity is not required. To see why, we look back at the outline of the proof that Γ is a contraction. Normal hyperbolicity is only used in the second step, to estimate $\mathrm{Lip}\{\Gamma \circ \sigma\}$ in terms of $\mathrm{Lip}\{\sigma\}$. In step two of the outline of the proof that Γ_D is a contraction, we estimated $\mathrm{Lip}\{\Gamma_D \circ \sigma\} \equiv \mathrm{Lip}\{I_p \circ \Gamma \circ \sigma\}$ using only the C^0 bound on $\Gamma \circ \sigma$ together with properties of I_p. Numerical experiments support the claim that the algorithm converges for attracting manifolds without normal hyperbolicity. Note: In the saddle case, the hypothesis that Σ be attracting may be replaced by the condition that Σ be 0–normally hyperbolic [9].

7   Conclusion and Future Work

The work reported in this paper had three stages: formulation of a method to locate invariant manifolds, testing the algorithm on examples, and proposing a mechanism for the observed convergence of the algorithm. Now we ask if the theoretical mechanism matches the observed behaviour of the algorithm.

First, the result shows that Γ_D is a contraction under the hypothesis that there exists an attracting manifold (normal hyperbolicity isn't required). This agrees with experience. For examples, see the Thom map and the sink map. Second, the convergence result indicates the contraction factor of Γ_D is close to $C_p\alpha$, where α is the contraction factor normal to Σ and C_p is a bound on the factor by which the C^0–norm of a function can grow under I_p. Experiments confirm that the contraction factor of Γ_D is directly proportional to α, for example, see the Thom map and the sink map. Also, in test cases, changes in the tangential exponential growth rate (and thus the normal hyperbolicity), had no effect on the contraction factor. Third, if $p = 1$, then $C_p = 1$, while if $p > 1$, then generally $C_p > 1$. This is because linear interpolation does not leave a convex neighborhood, but higher order interpolation may. Hence, if $\alpha \approx 1$, first order interpolation should be more likely to converge than higher order interpolation. This agrees with experience. For example, this happened with the Lorenz–84 torus. Fourth, in the result, if H is too small compared to ϵ, the Lipschitz constant of sections iterated under Γ_D may blow up. In practice, for some cases, (especially curves in $\mathbb{R}^3$), Γ_D did converge for large values of H, but not for smaller values of H – this is the subject of further tests.

The mechanism of convergence given by the result matches the experimental observations of the algorithm's behavior. If the result of Section 6 is an accurate model of the mechanism of convergence, does this model indicate any improvements to the algorithm? According to the result, the contraction factor is $C_p\alpha$. Ideally, $C_p = 1$, which means the set of sections whose graphs are contained in the neighborhood U of Σ is closed under I_p. Thus, it makes sense to modify I_p by cutting off the part of the graph of $I_p \circ \sigma$ outside of U. With this modification, $C_p = 1$ and the contraction factor of Γ_D is α, while the order of approximation is retained. Besides C_p, the other controllable parameter effecting convergence is C_p'. The bound on the Lipschitz constant of an interpolated section is $C_p'\epsilon/H$. A more robust algorithm can be obtained with interpolation schemes for which $C_p' > 0$ is small.

A natural extension of the algorithm is to compute 'parts' of manifolds. The extension to this case significantly widens the range of applicability of the method. This work is in progress, and preliminary results are promising. One topic this paper did not discuss was the computation of the hyperbolic splitting, although this splitting was computed at each continuation step in Examples 4 and 5. See [2] for details. From our experience, other areas which need work are the representation of the manifold at non–smooth points, better adaptive refinement schemes, and the problem of weak attraction.

8　Acknowledgements

9　References

[1] H. W. Broer, A. Hagen and G. Vegter, Finite element algorithms for invariant manifolds, in preparation.

[2] H. W. Broer, A. Hagen and G. Vegter, Finite element algorithms for invariant manifolds–the saddle case, in preparation.

[3] H. W. Broer, H. M. Osinga and G. Vegter, Algorithms for computing normally hyperbolic invariant manifolds , *Z. angew. Math. Phys.*, **48**, (1997) 480-524.

[4] P. G. Ciarlet and P.-A. Raviart, General Lagrange and Hermite interpolation in $\mathbb{R}^n$ with applications to finite element methods, *Arch. Rational Mech. Anal.*, **46**, (1972) 177-199.

[5] L. Dieci and J. Lorenz, Computation of invariant tori by the method of characteristics, *SIAM J. Numer. Anal.*, **32**, (1995) 1436-1474.

[6] N. Fenichel, Persistence and smoothness of invariant manifolds for flows, *Indiana Univ. Math. J.*, **21**, (1971/1972) 193-226.

[7] A. Hagen, Hyperbolic structures of time discretizations and the dependence on the time step, Ph.D. Thesis, University of Minnesota, 1996.

[8] M. W. Hirsch, Differential Topology, Springer-Verlag, New York, 1994.

[9] M. W. Hirsch, C. C. Pugh and M. Shub, Invariant Manifolds, Springer-Verlag, New York, 1977.

[10] Y. Kuznetsov, Elements of applied bifurcation theory, Springer-Verlag, New York, 1998.

[11] J. Palis and F. Takens, Hyperbolicity & sensitive chaotic dynamics at homoclinic bifurcations, Cambridge University Press, Cambridge, 1993.

[12] D. Ruelle, Elements of differentiable dynamics and bifurcation theory, Academic Press, Boston, 1989.

[13] A. Shil'nikov, G. Nicolis, and C. Nicolis, Bifurcation and predictability analysis of a low-order atmospheric circulation model, *Internat. J. Bifur. Chaos Appl. Sci. Engrg.*, **5**, (1995) 1701-1711.

[14] C. Sparrow, The Lorenz equations: bifurcations, chaos, and strange attractors, Springer-Verlag, New York, 1982.

[15] S. Wiggins, Normally hyperbolic invariant manifolds in dynamical systems, Springer-Verlag, New York, 1994.